HETU: a new high-resolution stress and texture neutron diffractometer at China Mianyang Research Reactor

Baihua Wang, Shengyi Zhong, Hao Lin, Arsen Goukassov, Zhaolong Yang, Jian Li, Guang-Ai Sun

JOURNAL OF APPLIED CRYSTALLOGRAPHY
ISSN 1600-5767

HETU: a new high-resolution stress and texture neutron diffractometer at China Mianyang Research Reactor

Baihua Wang,[a] Shengyi Zhong,[a]* Hao Lin,[a] Arsen Goukassov,[b] Zhaolong Yang,[c] Jian Li[c] and Guang-ai Sun[c]

[a]School of Materials Science and Engineering, Shanghai Jiao Tong University, Shanghai 200240, People's Republic of China, [b]Laboratoire Léon Brillouin (CEA-CNRS), CEA Saclay, Gif-sur-Yvette 91911, France, and [c]Key Laboratory of Neutron Physics and Institute of Nuclear Physics and Chemistry, China Academy of Engineering Physics, Mianyang 621999, People's Republic of China. *Correspondence e-mail: shengyi.zhong@sjtu.edu.cn

Received 17 July 2023
Accepted 9 October 2023

Edited by J. Keckes, Montanuniversität Leoben, Austria

Keywords: neutron diffractometers; residual stress; long-wavelength neutrons; instrument resolution.

HETU is a new high-resolution stress and texture neutron diffractometer installed at the C1 neutron guide at China Mianyang Research Reactor. The diffractometer is designed for precise residual stress and texture analysis of engineering components, as well as *in situ* investigations under various sample environments for engineering materials. The wavelength range of monochromatic incident neutrons is 1.634–5.800 Å, provided either by a double-focusing perfect single-crystal silicon monochromator in high instrument resolution mode or by a highly oriented pyrolytic graphite monochromator in high neutron flux mode. The intrinsic peak widths of HETU have been measured using a standard silicon powder sample, and residual stress measurements of an aluminium alloy shrink-fit ring and plug have been carried out. These results demonstrate that HETU is a reliable and appropriately designed diffractometer for promoting materials investigation.

1. Introduction

Neutron diffraction is one of the most powerful techniques for determining the stress and texture of engineering materials and components with high reliability and accuracy. This technique has been used in a variety of fields, including additive manufacturing (Fritsch *et al.*, 2021; Shen *et al.*, 2019), welding (Akrivos *et al.*, 2020; Goel *et al.*, 2020), and service and failure of materials (Withers, 2007). Advanced residual stress neutron diffractometers based on continuous wave (CW) neutron sources can be found at SALSA (Pirling *et al.*, 2006) at the Institute Laue–Langevin (ILL, Grenoble, France); DIANE [shut down at the end of October 2019 (Ceretti, 2000)] at Laboratoire Léon Brillouin (LLB, Saclay, France); STRESS-SPEC (Hofmann, Schneider *et al.*, 2006) at Heinz Maier-Leibnitz Zentrum (Garching, Germany); KOWARI (Kirstein, Luzin *et al.*, 2008; Brule & Kirstein, 2006) at the Australian Nuclear Science and Technology Organisation (Sydney, Australia); Residual Stress Instrument (RSI) (Moon *et al.*, 2002; Seong *et al.*, 2011) at the Korea Atomic Energy Research Institute (Daejeon, South Korea); Residual Stress Diffractometer (RSD) (Li *et al.*, 2014) at the China Advanced Research Reactor (CARR, Beijing, China); and Residual Stress Neutron diffractometer (RSND) (Li *et al.*, 2015, Mo *et al.*, 2018) at the China Mianyang Research Reactor (CMRR, Mianyang, China). Their performances are listed in Table 1. The number of residual-stress neutron diffractometers remains insufficient, and consequently, the number of experiments is limited. The construction of a high-

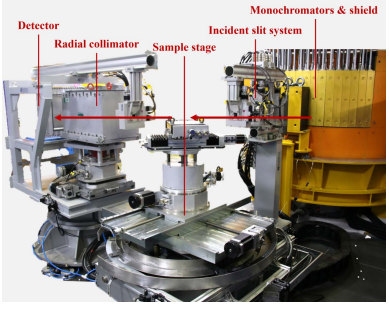

Table 1
Characteristics of neutron beam and instrument resolution of neutron diffractometers.

Name	Source	$\Delta d/d$	Monochromator	λ (Å)	Maximum flux (neutrons cm^{-2} s^{-1})
SALSA	ILL	–	Bent silicon	1.3–3.0	5.0×10^7
DIANE	LLB	1.9×10^{-3}	PG(002), PG(004)	2.3–6.0	3.8×10^6
STRESS-SPEC	FRM-II	2.0×10^{-3}	Ge(511), Si(400), PG(002)	1.0–2.4	3.5×10^7
KOWARI	OPAL	2.0×10^{-3}	Si(400)	1.2–2.8	7.0×10^6
RSI	HANARO	2.0×10^{-3}	Si(200), Si(311)	1.5–1.9	–
RSD	CARR	2.0×10^{-3}	Cu(220), Si(311)	0.9–2.7	2.7×10^7
RSND	CMRR	1.8×10^{-3}	Si(311), Si(511)	1.2–2.8	4.6×10^6

performance versatile residual-stress neutron diffractometer is required to alleviate this limitation and enable the measurement of many important engineering materials and components.

One issue concerns the neutron wavelengths and neutron flux at the sample position. The neutron flux decreases for wavelengths greater than the characteristic neutron wavelength of the thermal neutron spectrum according to the Maxwell distribution. Numerous efforts have been made to improve the neutron flux of long-wavelength neutrons at the sample position. One solution involves adopting a focusing monochromator at a cold neutron guide. The diffractometer DIANE (Ceretti, 2000) has adopted a pyrolytic graphite single crystal using the 004 or 002 reflection to provide the wavelength range 2.3–6.0 Å, allowing a good instrument resolution of 1.9×10^{-3} at a wavelength of 2.8 Å and a high neutron flux of 3.8×10^6 neutrons cm^{-2} s^{-1} at a wavelength of 3.0 Å. DIANE has demonstrated that the combination of a focusing monochromator and cold neutron beamline is a solution to mitigate the limitations of the stress diffractometer.

Further, to reliably and accurately separate close or overlapping diffraction patterns of dual or multi-phase materials, a high instrument resolution is required. The instrument resolution is determined by the properties of incident monochromatic neutron beams and the combination of neutron optics. To achieve high instrument resolution, it is essential to meticulously design neutron optics, including the monochromators, the slit system, the radial collimators and the detector.

A new high-resolution stress and texture neutron diffractometer – HETU – has been designed by the Neutron Science Research Center of Shanghai Jiao Tong University and built at the C1 cold neutron guide of the guide hall of the CMRR. Named after one of two mysterious patterns in ancient China, HETU represents exploration for materials science. To expand the capability to investigate engineering materials and components, a double-focusing perfect single-crystal silicon monochromator for high instrument resolution measurement mode and a highly oriented pyrolytic graphite (HOPG) monochromator for high neutron flux mode were selected. In addition, high-precision slit apertures, radial collimators and a high-resolution two-dimensional detector have been installed on HETU. Qilin – another stress diffractometer at CMRR (Li *et al.*, 2015), named after one of the sacred animals in ancient Chinese culture – and HETU are complementary diffractometers covering most engineering materials and components. Since HETU received its first neutron beam, several diffraction measurements have been performed to evaluate its performance. This paper describes the components of HETU and presents the results of some typical measurements.

2. Diffractometer components

2.1. Diffractometer layout and beam guide

At CMRR, the thermal neutrons from the reactor are moderated by a liquid hydrogen cold neutron source and then travel into the three neutron guides (C1, C2 and C3) of the

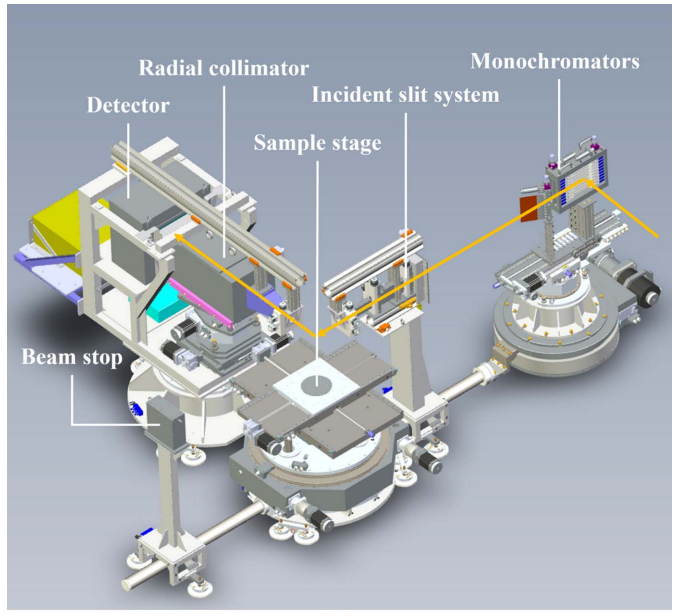

(*a*)

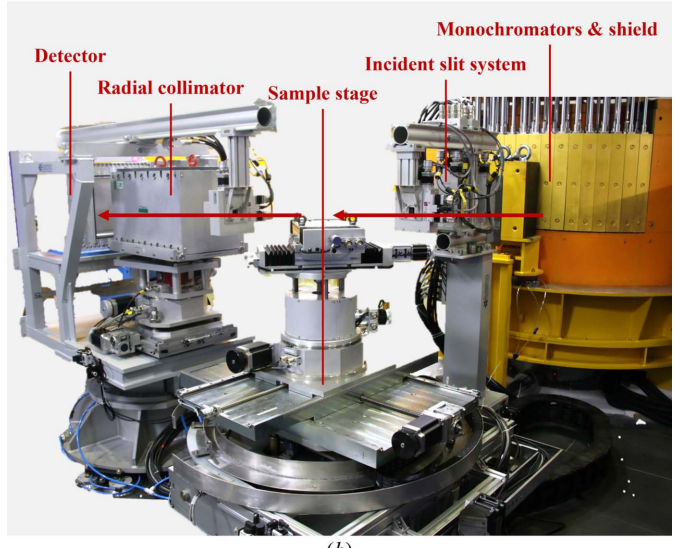

(*b*)

Figure 1
(*a*) Schematic and (*b*) photograph of the high-resolution stress and texture neutron diffractometer HETU at CMRR with the main components indicated.

guide hall. The HETU diffractometer was located at the midstream port of the C1 neutron guide, *i.e.* port C12. The C1 cold neutron guide consists of a curved guide with a length of 23.5 m and a radius of 2222.7 m, as well as numerous straight guide sections with a guide cross section of 30 × 200 mm (w × h) to transport a neutron beam with a characteristic neutron wavelength of 2.0 Å (Huo *et al.*, 2020). The curved guide efficiently prevents the delivery of high-energy neutrons and γ-rays from the neutron source to the instrument position, thereby improving the signal-to-noise ratio. Fig. 1 shows a schematic and a photograph of HETU with its main components indicated, which mainly consist of monochromators and their shielding, the incident slit system, sample stages, the diffracted beam slit, the radial collimator and the detector.

2.2. Monochromators

HETU has high instrument resolution and high neutron flux measurement modes, which are achieved by a silicon monochromator or an HOPG monochromator, as shown in Fig. 2. Two monochromators are mounted on the stage and are moved into and out of the beamline by motors.

2.2.1. Double-focusing perfect single-crystal silicon monochromator. For the high instrument resolution measurement mode, the silicon monochromator in double-focusing (vertical and horizontal) configuration provides a high-resolution monochromatic neutron beam with a resolution $\Delta\lambda/\lambda$ ranging from 0.5 to 1.0%, where $\Delta\lambda$ and λ are the full width at half-maximum (FWHM) and the wavelength of neutron beam, respectively. This resolution represents the ability to capture the variations in peak position of the neutron beam. The silicon monochromator consists of nine silicon monocrystal stacks with a length of 218 mm, a height of 21 mm and a thickness of 11.7 mm, each stack consisting of 13 silicon monocrystal wafers with a thickness of 0.9 mm. The single-crystal cut orientation is [100]. The symmetric 400 and asymmetric 311 reflections, with corresponding take-off angle ranges 74–120° and 90–120°, produce monochromatic neutron beams with wavelengths of 1.634–2.352 Å and 2.316–2.837 Å, respectively, which represent a good compromise for residual stress measurement in engineering materials (Table 2) at a sample scattering angle of $2\theta \simeq 90°$. According to the cold neutron spectrum of the C1 neutron guide (Huo *et al.*, 2020), the flux of neutrons with a wavelength less than 2.0 Å provided by HETU may be lower than that offered by thermal stress diffractometers such as Qilin (Li *et al.*, 2015). However, for wavelengths longer than 2.0 Å, HETU provides a better gain factor which results in a higher neutron flux. From this perspective, HETU is a superior option for materials that require longer-wavelength neutrons. The ranges of the horizontal and vertical focusing radii are 2200–4300 mm and 1800–3400 mm, respectively, corresponding to the monochromator-to-sample distance range 1700–2400 mm.

2.2.2. Highly oriented pyrolytic graphite monochromator. For high neutron flux mode, the HOPG monochromator provides a monochromatic neutron beam with $\Delta\lambda/\lambda$ from 1.0 to 12.0%. The HOPG monochromator consists of 45 pyrolytic graphite pieces of 22 × 22 × 2 mm in size which are welded on a single-crystal silicon wafer with indium. The reflections are 002 and 004, both of which have the take-off angle range 40–120° to produce monochromatic neutron beams in the wavelength ranges 2.291–5.800 Å and 1.145–2.900 Å, respectively. These cover the wavelengths of SiC (Matthey *et al.*, 2020; Xie *et al.*, 2017), ceramic (Fan *et al.*, 2017) and quartzite materials (Guezou *et al.*, 2021) (Table 2). However, the cold neutron spectrum indicates that the neutron flux may decrease for

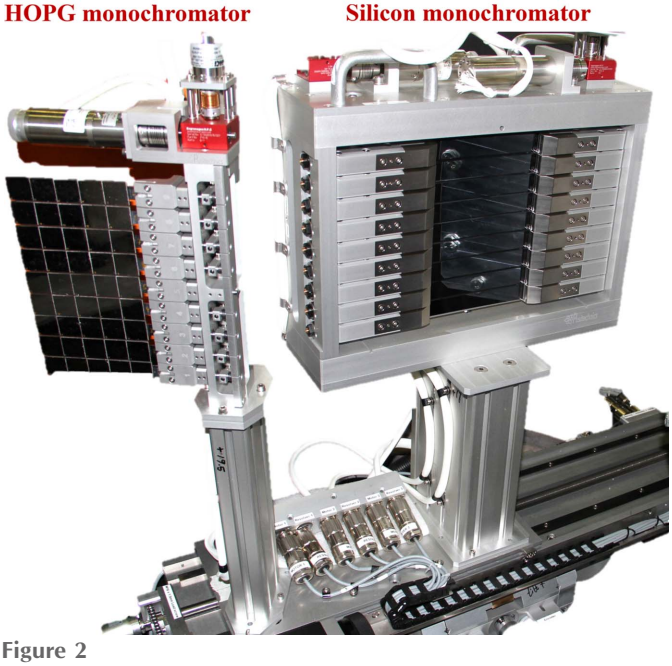

Figure 2
Double-focusing perfect single-crystal silicon monochromator and HOPG monochromator for the HETU diffractometer, installed on a stage for translation into the beam to select the high-resolution or high-flux measurement mode.

Table 2
Wavelength requirements to study some of the most suitable reflections for residual stress measurement at a scattering angle of 90°.

Material	Reflection (*hkl* or *hkil*)	*d* (Å)	λ (Å) (2θ~90°)
Al (f.c.c.)	111	2.329	3.3
	311	1.216	1.7
α-Fe	110	1.999	2.8
	211	1.154	1.6
γ-Fe	111	2.091	2.9
	311	1.092	1.6
Cu	111	2.087	2.9
	311	1.090	1.5
Ni	111	2.046	2.8
	31$\bar{1}$	1.063	1.5
Zircaloy	10$\bar{1}$2	1.332	1.9
	10$\bar{1}$3	1.131	1.6
Ti	10$\bar{1}$2	1.726	2.4
	10$\bar{1}$3	1.332	1.9
SiC	1$\bar{1}$00	2.651	3.7
	11$\bar{2}$0	1.535	2.2
α-Al_2O_3	006	2.165	3.1
	300	1.372	1.9
ZrO_2	111	2.938	4.1
	31$\bar{1}$	1.534	2.2
Quartzite (α-SiO_2)	10$\bar{1}$0	3.323	4.7

wavelengths below 1.5 Å and above 5.5 Å, to approximately the order of 10^5. Therefore, experiments carried out at these wavelengths present significant challenges.

2.3. Incident slit system

The divergence and the cross section of the incident monochromatic neutron beam are related to the instrument resolution and gauge volume definition, respectively. Three slits made of 2 mm-thick tungsten carbide blades coated with Gd are used to adjust the beam divergence and define the cross-section size of the incident beam. The maximum cross section is 30 × 100 mm for the first slit (slit-I) and the second slit (slit-II), and 30 × 30 mm for the third slit (slit-III). The distance between slit-I and slit-II is 500 mm, and the distance between slit-II and slit-III can be adjusted along an aluminium alloy rod. The minimum distance from slit-III to the centre of the gauge volume is 200 mm. Slit-III defines the gauge volume, while slit-I and slit-II predominantly eliminate neutrons with significant divergence to improve instrument resolution and diminish the background. The entire incident slit system is mounted on a connecting rod between monochromators and sample stages and can be moved. The cross section is automatically adjusted by motors with a high accuracy of ±1 µm each to achieve precise control of the beam divergence and cross-section size.

2.4. Sample stages

2.4.1. Main sample stage. The reliability and positioning precision of the sample stage are critical for measuring the residual stress of large engineering components. A main sample stage was designed with a sample space of 600 mm radius and a maximum load capacity of 1000 kg to accommodate large engineering components and sample environment devices for *in situ* experiments. This stage has functions of rotation, translation along the X and Y axes within a range of −300 to 300 mm, and lifting along the Z axis within a range of 0 to 500 mm, with a movement accuracy of ±100 µm. Even when large engineering components are not positioned at the centre of the main sample stage, *i.e.* the centre of gravity of the component is not at the centre of the stage, the movement accuracy of the Z axis remains at ±200 µm, enabling sufficient accuracy in positioning of the gauge volume.

2.4.2. Small sample stage. In addition to the main sample stage, a small sample stage was designed. The small sample stage can be easily installed on or removed from the main sample stage and has a maximum load capacity of 10 kg. It also has the ability to rotate, translate along the X and Y axes within the range −50 to 50 mm, and lift along the Z axis within the range 0 to 100 mm, each with a movement accuracy of ±10 µm. This stage offers higher positioning precision than the main sample stage and is used for measuring small engineering materials and components.

2.4.3. Eulerian cradle. Texture analysis of engineering materials is also an important area of investigation. A special Eulerian cradle was developed for HETU with a load capacity of 5 kg. In addition to the φ rotation axis, with an accuracy of 0.008°, and the χ tilt axis, with an accuracy of 0.01°, it has X, Y and Z axes for precise positioning with an accuracy of ±10 µm. An automatic sample changer for texture analysis has been developed that can mount ten samples for automated measurement, improving beam utilization.

2.5. Radial collimator

The gauge volume, which is the intersection of the incident and diffracted beams, is crucial for the reliability and accuracy of neutron diffraction residual stress measurements. Two radial collimators from Euro Collimators were selected with divergent resolutions of 0.1 and 0.2° in the horizontal direction. Combined with an inner radius of 600 mm and a length of 600 mm, they provide FWHMs of the gauge volumes of 2 and 4 mm, respectively. The collimator blades are made of PET foils coated on both sides with 0.025 mm Gd_2O_3 to effectively absorb stray neutrons and improve the signal-to-noise ratio of diffraction patterns. An oscillating stage at the bottom of the collimator avoids dead zones in diffraction patterns by oscillation. Translation axes, perpendicular and parallel to the diffracted beam, shift the centre of the radial collimator to keep it coincident with the centre of the gauge volume by collimator oscillation.

2.6. High-resolution 2D detector

^{3}He-based neutron detectors have low sensitivity to gamma radiation background generated by the neutron source and at the instrument. Therefore, a novel ^{3}He two-dimensional position-sensitive detector from DENEX is used on HETU to collect diffraction patterns. This detector covers Bragg angles from 30 to 130° with a kinematic accuracy of 0.009°. The effective detection size of the detector is 300 × 300 mm with a position resolution of 1 × 2 mm (h × v). The detector efficiency for 2.0 Å neutrons is better than 70%. The detector is divided into 256 × 256 pixels. The pixel width of the centre region (100 × 100 mm) of the detector is approximately 0.9621 mm at a sample-to-detector distance of 1500 mm, determined by varying the detector Bragg angle at equal intervals to measure the identical diffraction peak of the α-Fe steel pin.

2.7. Sample environments

Investigation of the deformation process of engineering materials under various sample environments is also one of the important objectives of HETU. For this purpose, the HETU team has developed sample environment devices including mechanical loading and heating/cooling systems. The mechanical loading system enables tension and compression with a maximum loading force of 15 kN. The thermal sample environments cover low and high temperatures, with low temperatures ranging from 93.15 to 298.15 K and high temperatures ranging from 298.15 to 1273.15 K with an accuracy of ±5 K. These sample environments meet the requirements for simulating the processing or service loads of most materials. Meanwhile, devices for torsion and tension with χ and φ angles are under development to provide simultaneous strain/stress and texture measurements.

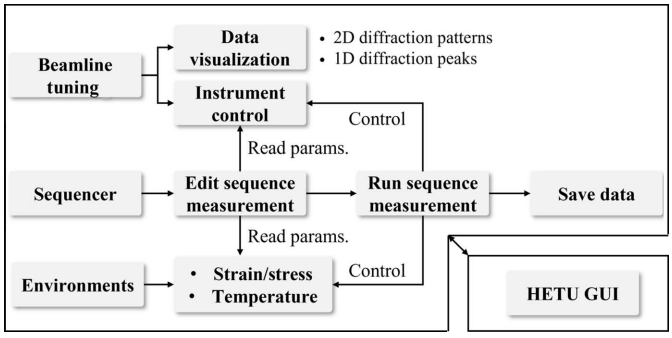

Figure 3
Concept of instrument control software package *HETU GUI* for HETU.

3. Control program and data processing

3.1. *HETU GUI*

The instrument is controlled using *HETU GUI*, a program based on *Labview*, developed for HETU to provide instrument control, status overview and data acquisition, and experiment workflows. The concept of *HETU GUI* is shown in Fig. 3. The *Beam Tuning* interface displays the diffraction patterns of the detector and diffraction peaks, as well as the status of each axis of HETU. This interface is also used to adjust the position of each axis. The *Sequencer* interface provides a multi-measure workflow that is user-friendly, allowing experimenters to simply fill in a measurement list and set sample instrument configurations. The workflow was designed with flexibility for more complicated setups. Loops can be added to measure the same sample at different times, which is very convenient for automatic residual stress measurements and *in situ* experiments. Users can choose to count on the basis of time, beam monitor count or total detector count. The *Environment* interface can be invoked from *Sequencer* to facilitate *in situ* experiments by monitoring and modifying the parameters of sample environment devices.

3.2. *HRTex*: texture data processing tool

The general texture data processing tool *HRTex* was developed by Yang *et al.* (2022) for monochromatic neutron diffraction of stress and texture neutron diffractometers based on CW neutron sources. This program processes the raw data of the 2D detector for each pixel and projects the intensity of each pixel directly onto a pole figure, with the aim of improving of the resolution and accuracy of pole figure calculations. With these features, *HRTex* can capture the high-resolution details of complex texture patterns. *HRTex* is freely available and can be found at https://neutron.sjtu.edu.cn.

4. Examples of measurements

4.1. Neutron flux at the sample position

The neutron flux at the sample position is crucial for both the detection efficiency and the signal-to-noise ratio of diffraction patterns. To determine the neutron flux with optimal monochromator focusing conditions, a neutron

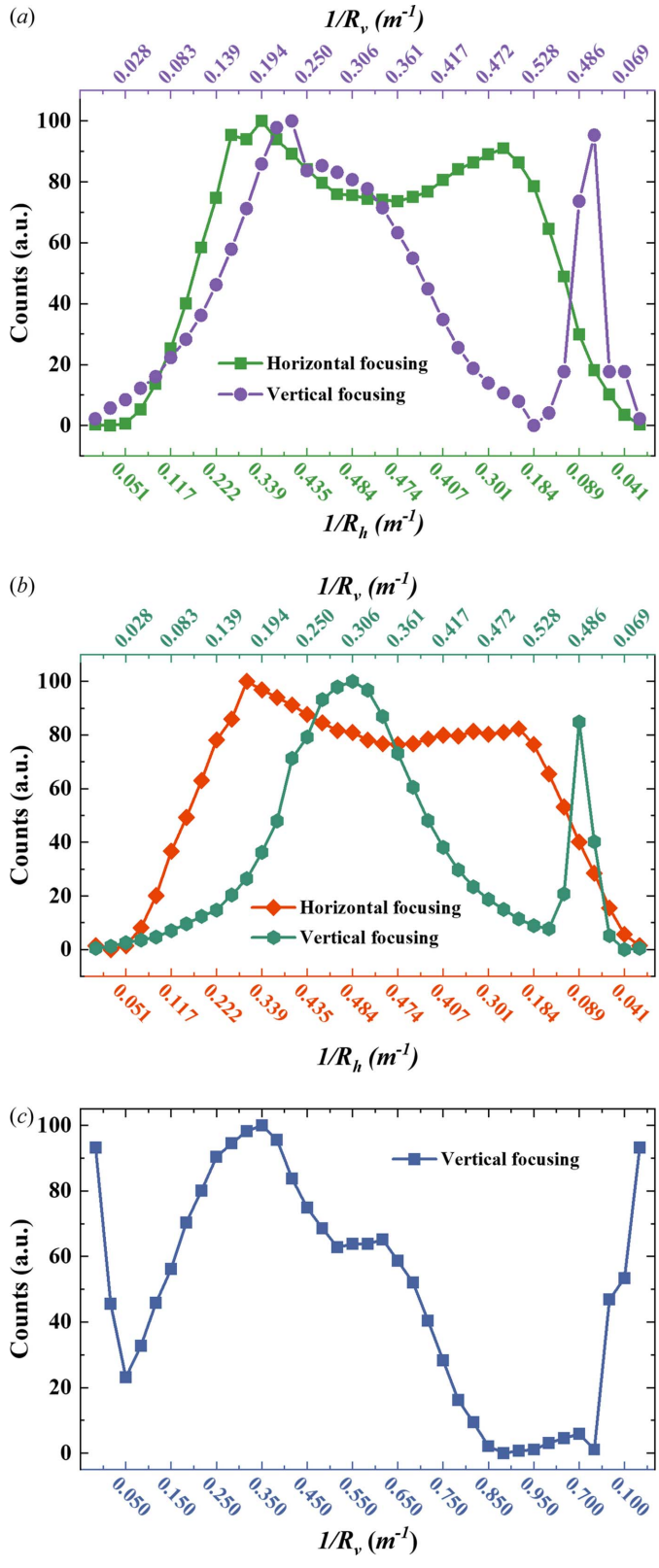

Figure 4
ROI counts of the neutron camera at the sample position as a function of the reciprocal of the horizontal (R_h) or vertical (R_v) focusing radius. The scale numbers on the horizontal axes increase and subsequently decrease implying a cyclical variation in the focusing radius. (*a*) Si(400) monochromator. (*b*) Si(311) monochromator. (*c*) HOPG monochromator.

camera was utilized to image the beam and calculate counts of the region of interest (ROI) as a function of vertical and horizontal focusing radii of the monochromators when the take-off angle of the monochromators was set to $2\theta \simeq 90^\circ$, as shown in Fig. 4. The ROI measured 5 × 5 mm and was located at the centre of the neutron spot image. The distance between the neutron camera and the monochromators was 2100 mm. As the neutron camera detects relative brightness, the counts were normalized and the horizontal axis was set to represent the horizontal or vertical focusing radii of monochromator. On the basis of these results, an optimal focusing radius was selected and the neutron flux at the sample position was measured using the gold foil activation method.

4.1.1. Neutron flux from the silicon monochromator. The neutron flux values at the sample position are 3.41×10^6 and 5.76×10^6 neutrons $cm^{-2}\ s^{-1}$ for neutrons with wavelengths of 1.920 and 2.319 Å, respectively, reflected by Si(400) and Si(311) at a take-off angle of $2\theta \simeq 90^\circ$. From Figs. 4(*a*) and 4(*b*), the optimal vertical and horizontal focusing radii of Si(400) are 4320 and 2950 mm, whereas those of Si(311) are 3272 and 3326 mm, respectively. Note that there is an additional maximum ROI count in the later part of the vertical focusing curve. This could be due to the presence of a focusing radius near the optimal value. Theoretically, the vertical and horizontal focusing radii should be identical for Si(400) and Si(311) at the same take-off angle. However, there are some differences in these tests, possibly due to asymmetric reflection in Si(311) (Seong *et al.*, 2010; Mikula *et al.*, 2014). These results indicate that the neutron flux at the sample position is comparable to that of other neutron diffractometers.

4.1.2. Neutron flux from the HOPG monochromator. At a take-off angle of $2\theta \simeq 90^\circ$, HOPG(002) and (004) reflect neutrons with wavelengths of 4.742 and 2.371 Å, respectively, due to the secondary diffraction exhibited by pyrolytic graphite. Both contribute to the neutron flux, resulting in a value of 3.01×10^7 neutrons $cm^{-2}\ s^{-1}$ at the sample position. These results were obtained under conditions where the vertical focusing radius was optimized to 2857 mm. As shown in Fig. 4(*c*), there is an additional maximum count for a reason similar to that described for the silicon monochromator. The neutron flux reflected by HOPG is approximately 6× that of a silicon monochromator, providing a high neutron flux.

4.2. Peak widths and instrument resolution

The peak widths and the instrument resolution $\Delta d/d$ of a diffractometer are important indicators of its performance. The peak widths of HETU were measured using the NIST SRM 640F standard silicon powder sample and the instrument resolution was calculated using the equation $\Delta d/d = \frac{1}{2}\mathrm{FWHM}\cot\theta$, where FWHM and θ are the FWHM of the diffraction peaks and half the Bragg angle, respectively. The silicon powder was packed into a vanadium cylinder with a diameter of 5 mm and a height of 50 mm. In this measurement, the monochromatic neutron wavelength was 2.319 Å, obtained with the Si(311) reflection at a take-off angle of $2\theta \simeq 90^\circ$. The monochromator-to-sample and sample-to-detector distances were 2100 and 1500 mm, respectively. The gauge volume was 4 × 4 × 4 mm, determined by slit-III with a cross section of 4 × 4 mm and a radial collimator with an FWHM of the gauge volume of 4 mm. The (111), (220), (311) and (400) lattices planes of the silicon powder were measured, and the peak-width function and instrument resolution are shown in Fig. 5. The data for other diffractometers in the figure are taken from the literature (Kirstein, Brule *et al.*, 2008; Ceretti, 2000; Hofmann, Seidl *et al.*, 2006). The figure shows that HETU has a narrow peak width and superior instrument resolution, with an optimal FWHM of 0.22° and an optimal instrument resolution of $\Delta d/d = 1.9 \times 10^{-3}$ without deducting diffraction broadening caused by the sample size. These results demonstrate the high-resolution nature of the cold neutron beam and validate the conceptual design of HETU for high instrument resolution. The instrument resolution of a continuous beam diffractometer is given by (Hutchings, 2005)

$$(\Delta d/d)^2 = (\cot\theta^{\mathrm{s}}\Delta\theta^{\mathrm{s}})^2 + (\cot\theta^{\mathrm{M}}\Delta\theta^{\mathrm{M}})^2, \qquad (1)$$

where θ^{M} and θ^{s} are the Bragg angle of the monochromator and the diffraction angle of the sample, respectively; $\cot\theta^{\mathrm{s}}\Delta\theta^{\mathrm{s}}$

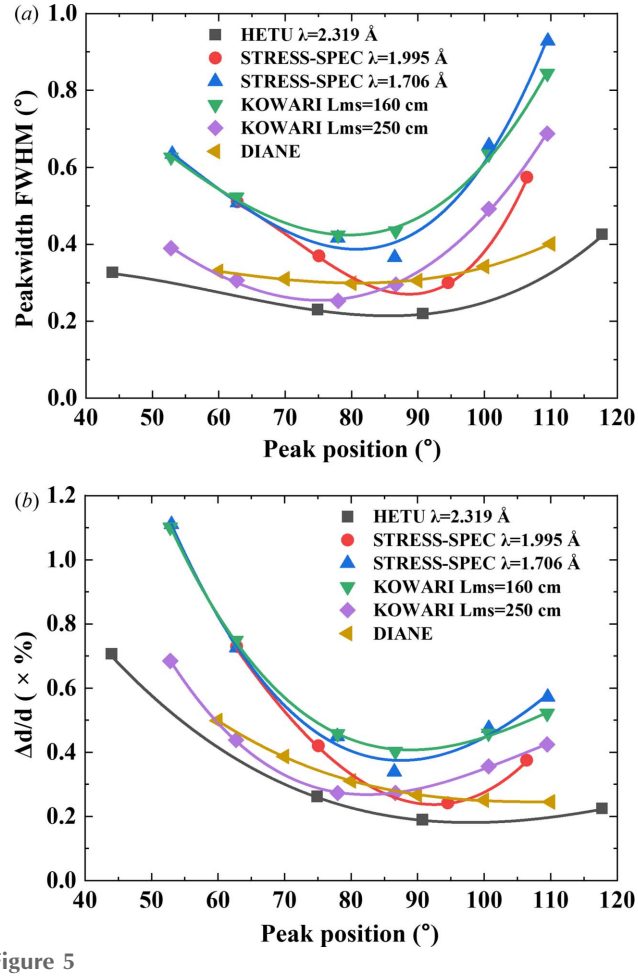

Figure 5
Instrument resolution of HETU as a function of the Bragg angle 2θ for a wavelength of 2.319 Å using Si(311), compared with experimental results from other stress diffractometers; the KOWARI data are Monte Carlo simulation results. (*a*) Peak width function of the diffraction peaks. (*b*) Instrument resolution function calculated from the FWHM.

is the divergence in the diffraction plane of the diffracted beam with respect to the incident beam, contributing to the instrument resolution, and $\cot\theta^{M}\Delta\theta^{M}$ is the relative peak width of the incident monochromatic beam. For HETU, $\cot\theta^{s}\Delta\theta^{s}$ decreases on increasing the monochromator-to-sample and sample-to-detector distances. Further, the silicon monochromator provides a relatively narrow peak width and long-wavelength neutrons to decrease $\cot\theta^{M}\Delta\theta^{M}$. These two factors improve the resolution of HETU. In this case, the relative peak width contributes to the resolution more than the beam divergence from the view point of the magnitude of the two terms. With these peak widths of HETU, neutron diffraction line profile analysis can be performed.

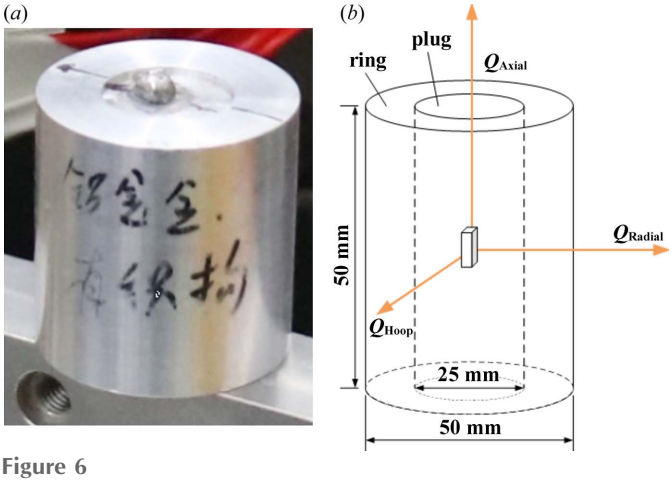

Figure 6
Shrink-fit ring and plug of aluminium alloy. (*a*) Photograph and (*b*) schematic of the ring and plug.

4.3. Measurement of residual stress in a shrink-fit ring and plug of aluminium alloy

Neutron diffraction measurement of residual stress in an aluminium alloy shrink-fit ring and plug is an important part of verifying the reliability of a stress neutron diffractometer. This measurement was originally undertaken under the auspices of the Versailles Project on the Advanced Materials and Standards Technical Working Area 20 (VAMAS TWA 20) and was performed at 18 neutron sources (Webster, 2000; Daymond *et al.*, 2002). Referring to VAMAS, the specially manufactured ring and plug duplicated specimen have a height of 50 mm and

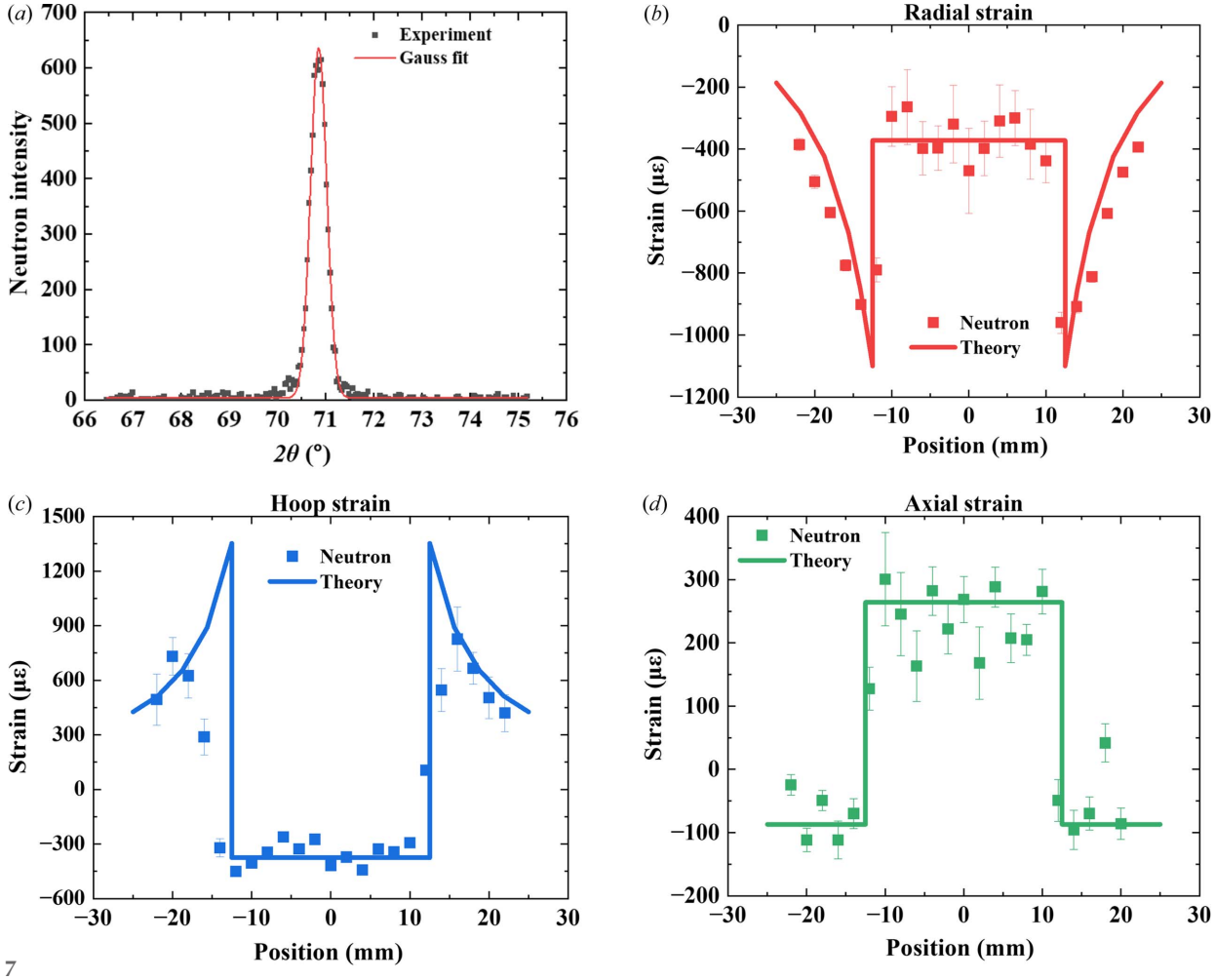

Figure 7
Residual strain of the (200) lattice plane of the shrink-fit ring and plug of aluminium alloy compared with the theoretical results. (*a*) Diffraction peak of the (200) lattice plane and its Gaussian fit curve to illustrate the data processing. Residual strain in the (*b*) radial direction, (*c*) hoop direction and (*d*) axial direction.

nominal outer diameters of 50 and 25 mm, respectively. The outer diameter of the plug was designed to be 0.03 mm larger than the inner diameter of the ring to give a nominal radial interference of 0.015 mm. The plug was placed in liquid nitrogen and allowed to equilibrate, then rapidly removed from the liquid nitrogen and inserted into the ring. There its thermal expansion was restricted by the smaller inner diameter of the ring, which generated residual stress. The ring and plug specimen are shown in Fig. 6.

The strains in the radial, hoop and axial directions of this aluminium alloy shrink-fit ring and plug were measured at HETU. The incident beam wavelength was 2.319 Å. The monochromator-to-sample and sample-to-detector distances were 2100 and 1500 mm, respectively. For both the radial and the hoop direction measurements, the gauge volume was set to $2 \times 2 \times 10$ mm. For the axial orientation, the gauge volume was $2 \times 2 \times 2$ mm. The 200 reflection was then measured at a Bragg angle of $2\theta \simeq 70.818^\circ$. The edges of the sample were scanned to determine the centre of the sample first for each measurement orientation. Strains along the specimen diameter were measured with a step displacement of 2 mm. Finally, the stress-free reference d_0 was determined for all three orientations by measuring the reference plug. The strain was calculated using $\varepsilon = (d - d_0)/d_0$, where d and d_0 are the 'stress' and 'stress-free' lattice spacings. Fig. 7 shows the measured results and compares them with the theoretical results obtained using the Bayesian approach (Webster, 2000; Daymond *et al.*, 2002). The variation trends of radial and hoop strains are consistent with the theoretical values. However, the axial data have greater scatter than the hoop and radial directions. This could be attributed to statistical quality, specifically the peak heights and widths of the raw data. Alternatively, the statistical quality may stem from the expanded gauge volume and reduced neutron flux resulting from the longer path of neutrons when measuring axial strain. It is advisable to use a smaller gauge volume and a longer measurement time for the axial direction, as suggested in VAMAS. These results are consistent with previous studies (Webster, 2000; Daymond *et al.*, 2002; Hao *et al.*, 2023) that have illustrated the feasibility and accuracy of HETU.

5. Conclusions

The new stress and texture neutron diffractometer, HETU, has been installed at CMRR. It incorporates a double-focusing silicon monochromator and an HOPG monochromator that can be used in high instrument resolution or high neutron flux measurement mode. A series of carefully designed neutron optics were aimed at achieving high instrument resolution. Measurement of the peak width function demonstrated that the design for high instrument resolution was successful for HETU. Specifically, the relatively narrow peak widths of the incident neutron beam and the long-wavelength neutrons provided by the silicon monochromator mainly contribute to the high resolution. Measurement of an aluminium alloy shrink-fit ring and plug showed that HETU has sufficient reliability to measure the residual stress of engineering materials and components. The texture measurements will be carried out as part of the validation of the HETU capability. These results indicate that the main aim of HETU has been achieved. The general user programme has already started and the devices described in this paper are available for this programme.

Funding information

This work is supported by the National Key Research and Development Programme of China (grant No. 2021YFA1600900).

References

Akrivos, V., Wimpory, R. C., Hofmann, M., Stewart, B., Muransky, O., Smith, M. C. & Bouchard, J. (2020). *J. Appl. Cryst.* **53**, 1181–1194.
Brule, A. & Kirstein, O. (2006). *Physica B*, **385–386**, 1040–1042.
Ceretti, M. (2000). *Physica B*, **276–278**, 932–933.
Daymond, M. R., Johnson, M. W. & Sivia, D. S. (2002). *J. Strain Anal. Eng. Des.* **37**, 73–85.
Fan, K., Ruiz-Hervias, J., Pastor, J. Y., Gurauskis, J. & Baudín, C. (2017). *Int. J. Refract. Met. Hard Mater.* **64**, 122–134.
Fritsch, T., Sprengel, M., Evans, A., Farahbod-Sternahl, L., Saliwan-Neumann, R., Hofmann, M. & Bruno, G. (2021). *J. Appl. Cryst.* **54**, 228–236.
Goel, S., Neikter, M., Capek, J., Polatidis, E., Colliander, M. H., Joshi, S. & Pederson, R. (2020). *Mater. Des.* **195**, 109045.
Guezou, J. C., Azzeddine, H., Ceretti, M. & Baudin, T. (2021). *Geol. J.* **57**, 1125–1136.
Hao, J., Tan, Z., Lu, H., Deng, S., Shen, F., Zhao, D., Zheng, H., Ma, Q., Chen, J. & He, L. (2023). *Nucl. Instrum. Methods Phys. Res. A*, **1055**, 168532.
Hofmann, M., Schneider, R., Seidl, G. A., Rebelo-Kornmeier, J., Wimpory, R. C., Garbe, U. & Brokmeier, H. (2006). *Physica B*, **385–386**, 1035–1037.
Hofmann, M., Seidl, G. A., Rebelo-Kornmeier, J., Garbe, U., Schneider, R., Wimpory, R. C., Wasmuth, U. & Noster, U. (2006). *Mater. Sci. Forum*, **524–525**, 211–216.
Huo, H., Li, H., Wu, Y., Zhu, S., Liu, B., Sun, Y., Wang, S., Cao, C., Yin, W., Tang, B. & Rogers, J. (2020). *Nucl. Instrum. Methods Phys. Res. A*, **953**, 163063.
Hutchings, M. T. (2005). *Introduction to the Characterization of Residual Stress by Neutron Diffraction.* Boca Raton: CRC Press.
Kirstein, O., Brule, A., Nguyen, H. & Luzin, V. (2008). *Mater. Sci. Forum*, **571–572**, 213–217.
Kirstein, O., Luzin, V., Brule, A., Nguyen, H. & Tawfik, D. (2008). *Adv. Mater. Res.* **41–42**, 439–444.
Li, J., Wang, H., Sun, G., Chen, B., Chen, Y., Pang, B., Zhang, Y., Wang, Y., Zhang, C., Gong, J. & Liu, Y. (2015). *Nucl. Instrum. Methods Phys. Res. A*, **783**, 76–79.
Li, J. H., Liu, Y. T., Gao, J. B., Hu, R., Liu, R. D., Sun, S., Li, J. Z. & Chen, D. F. (2014). *Mater. Sci. Forum*, **777**, 161–164.
Matthey, B., Pirling, T., Herrmann, M. & Schreiber, J. (2020). *J. Eur. Ceram. Soc.* **40**, 1035–1042.
Mikula, P., Vrána, M., Pilch, J., Seok Seong, B., Woo, W. & Em, V. (2014). *J. Appl. Cryst.* **47**, 599–605.
Mo, F., Sun, G., Li, J., Zhang, C., Wang, H., Chen, Y., Liu, Z., Yang, Z., Li, H., Yan, Z., Pang, B., Huang, Y. Tian, Y., Gong, J., Chen, B. & Peng, S. (2018). *Quantum Beam Sci.* **2**, 15.
Moon, M. K., Lee, C. H., Em, V. T. & Kim, H. (2002). *Appl. Phys. Mater. Sci. Process.* **74**, s1437–s1439.
Pirling, T., Bruno, G. & Withers, P. J. (2006). *Mater. Sci. Eng. A*, **437**, 139–144.
Seong, B.-S., Em, V., Mikula, P., Šaroun, J. & Kang, M.-H. (2010). *J. Appl. Cryst.* **43**, 654–658.

Seong, B. S., Em, V. T., Mikula, P., Šaroun, J. & Kang, M. H. (2011). *Mater. Sci. Forum*, **681**, 426–430.
Shen, C., Reid, M., Liss, K., Pan, Z., Ma, Y., Cuiuri, D., van Duin, S. & Li, H. (2019). *Addit. Manuf.* **29**, 100774.
Webster, G. A. (2000). *Neutron Diffraction Measurements of Residual Stress in a Shrink-Fit Ring and Plug.* National Physical Laboratory.
Withers, P. J. (2007). *Rep. Prog. Phys.* **70**, 2211–2264.
Xie, X., Hu, X., Chen, X., Liu, F., Yang, X., Xu, X., Wang, H., Li, J., Yu, P. & Wang, R. (2017). *CrystEngComm*, **19**, 6527–6532.
Yang, J., Zhong, S., Luzin, V., Li, J., Liu, X. & Dan, C. (2022). *J. Appl. Cryst.* **55**, 425–435.